Plasmon dynamics of nanosystems on femtosecond timescales

Final report on the results of project FK128077

2022

Dr. Zsuzsanna Pápa

Introduction

Electromagnetic field enhancement is a fundamental consequence of surface plasmon generation exploited in numerous scientific and technological applications [1-10]. This phenomenon inherently goes together with the nanoscale spatial localization of optical fields, i.e. the exciting laser field. In addition, if plasmons are excited with few-cycle laser pulses, not only previously inaccessible spatial dimensions open up, but also very short timescales, allowing for spatiotemporal control of optical interactions on a nanometer and few-femtosecond scale [11-18]. Validated experimental techniques exist to gain either information about the field enhancement [19-21] or the near-field dynamics of plasmonic nanostructures [22-26]. However, there are still a lot to explore regarding *the temporal properties of the plasmonic fields and their optical control*. For example, detailed analysis of the possibility to excite few-cycle localized surface plasmon fields at nanoparticles by ultrashort few-cycle laser pulses is lacking. Moreover, if these short plasmonic transients can be combined with large field enhancement factors, new paths can open up for ultrafast optoelectronic devices. Different, previously not widely studied aspects can be revealed about elementary excitation processes by monitoring charge dynamics during plasmon excitation in fs-timescales.

Along these considerations, in my research plan submitted in 2018, I highlighted **three main topics** to contribute: **1) determination of plasmonic field enhancement** in application-oriented samples, **2)** revealing different aspects of **few-femtosecond plasmon dynamics**, and **3)** monitoring **plasmon-associated charge dynamics** with ellipsometry (noted as sections 2.1, 2.2 and 2.3 in the research plan, respectively). In the following sections, I will summarize the most important results and scientific outputs of my research in these fields.

Results

1) Determination of plasmonic field enhancement in application-oriented samples

Our first experiments aiming the determination of field enhancement factors and exploring the limitations of our previously published method [20] were carried out on plasmonic nanotriangles, where plasmonic hot-spots at sharp corners with higher field enhancement are expected to emerge. During these measurements, an interesting damage effect was observed, which turned out to be very important for the correct interpretation of the measured electron signal and the achievable field enhancement factors. In more detail, *we observed the evolution of femtosecond breakdown of lithographically produced plasmonic nanoparticles* with increasing laser intensity. In our experiments, localized plasmons were generated with 40-fs laser pulses in nanotriangle arrays. The morphology of this periodic array changed gradually with intensity, ranging from stochastic nanoparticle removal to laser nanolithography of the underlying substrate material. We demonstrated and supported with simulation results that the ultrafast breakdown phenomenon first appeared at plasmonic hot-spots of the triangular nanoparticles. Based on these observations we could also derive the damage threshold value of these plasmonic nanoparticle arrays [27]. These results help to identify the appropriate intensity regimes where our field enhancement measurement technique provides reliable results. However, choosing the appropriate intensity regime does not mean solely to avoid the damage of the nanoparticles.

A very important requirement of our field enhancement measurement technique is the application of high laser intensities, since our method is only valid in the so-called strong-field regime (for a review of strong-field effects see [28]). Certain substrates that are used for nanoparticle fabrication can also become modified/damaged due to plasmonic effects if they are exposed to high intensity laser pulses during the experiments, which should be explored and taken into account during the planning of the applied experimental parameters.

These effects were studied on laser irradiated surfaces in collaboration with the Max Born Institute, in Germany. An optical imaging system was designed that enables us to observe the formation of periodic nanopatterns on the sample surface. We demonstrated that the characteristic fringe pattern appearing in the backscattered light can be attributed to the surface modification, providing *an in-situ tool for monitoring the surface quality during experiments performed with fs-lasers* [29].

A similar *surface modification was observed during our experiments in the infrared (IR) spectral range* [30]. The near-IR (NIR) to IR regime is particularly interesting from the point of view of photoemission processes, since transition to strong-field regime depends on not only the applied laser intensity but also the applied wavelengths [31, 32]. Using IR pulses, strong-field effects can be accessed at lower intensities by exploiting nanoscale plasmonic field confinement, enhancement and ponderomotive wavelength scaling at the same time [33]. By applying a variable wavelength IR source, we planned to analyze these intensity/wavelength scaling laws of photoemission in detail. As a first step, we investigated the interaction of the indium-tin-oxide (ITO) layer (commonly used conductive layer in nanoplasmonic experiments) with the femtosecond IR pulses. Using pulses between 1.6 and 2.4 μm central wavelengths, we observed robust periodic surface morphologies on the ITO surface. Supporting finite-difference time-domain (FDTD) calculations suggests that the surface forms are *rooted in the plasmonic field localization in the surface pits* leading to a periodically increased absorption of the laser pulse energy that creates the observed periodic structures. Based on these experiments we could identify the threshold intensities of different surface modifications. For our ongoing investigations including also the plasmonic nanoparticles laying on the surface of the ITO, these are very important input parameters for the correct conduction of the experiments.

In another measurement campaign, we aimed at the ultrafast control of plasmonic field enhancement. To demonstrate the possibility of ultrafast tuning of the field enhancement factor appearing on a given nanostructured sample, we carried out photoelectron spectroscopic measurements on nanorods with different lengths, i.e. different plasmonic resonance properties. For the illumination, we applied 30-fs laser pulses in the NIR spectral range with either linear or circular polarization states. We could demonstrate that *by changing the polarization state of the illumination, we are able to select the excitation of different plasmonic modes resulting in large differences in the achievable field enhancement factors* [34]. With circularly polarized pulses, the appearing field enhancement factors depend on not only the excitation of multiple plasmonic modes, but also the phase relations between them. For nanorods with length being nearly twice the width, the circularly polarized illumination allows for the in-phase superposition of the plasmonic modes resulting in large field enhancement. This simple mode-mixing property provides an extra knob for the ultrafast control the near-field of plasmonic nanorods. A further benefit of this method is that it can be established easily in experiments and can be further exploited in diverse applications like helicity-driven optical switches with purpose-designed nanostructures.

2) Revealing different aspects of few-femtosecond plasmon dynamics

One of the main goals of the project is to investigate the possibility to generate few-cycle plasmonic fields with few-cycle laser pulses. For such an experiment, purpose-designed samples are needed. A widely applied plasmonic sample type contains nanoparticles forming a periodic array. It is known, that the coupling between the electric fields of these nanoparticles can affect the plasmonic properties of the ensemble, depending on the particle configuration [35]. In our research article [36] we investigated the effect of plasmonic resonance properties on the temporal response and field enhancement property of the nanoparticle arrays. By systematically *changing the lattice constant for arrays containing identical metal nanorods*, we experimentally demonstrated how grating-induced effects affect the position and, more importantly, the broadening of plasmonic resonance spectra. We correlated these changes with the achievable field enhancement and the temporal duration of plasmon transients and *formulated criteria for the generation of enhanced few-cycle localized plasmon oscillations*.

As a continuation of the project, we are working on the *experimental observation of short plasmon transients with a method based on electron-autocorrelation measurements*. For the experiments, we used a broadband Ti:S oscillator providing ultrashort, few-cycle laser pulses (5.5 fs) and a dispersion-balanced Michelson interferometer to produce two time-delayed pulses. These pulses are focused to the nanoplasmonic sample in the vacuum chamber (Fig. 1 a)). With this setup, the total plasmonic photocurrent can be measured with the electron spectrometer as a function of the delay between the pulses. Since the photoemission process is induced by the plasmonic near field, it is possible to estimate on the length of excited plasmon field from the recorded autocorrelation function.

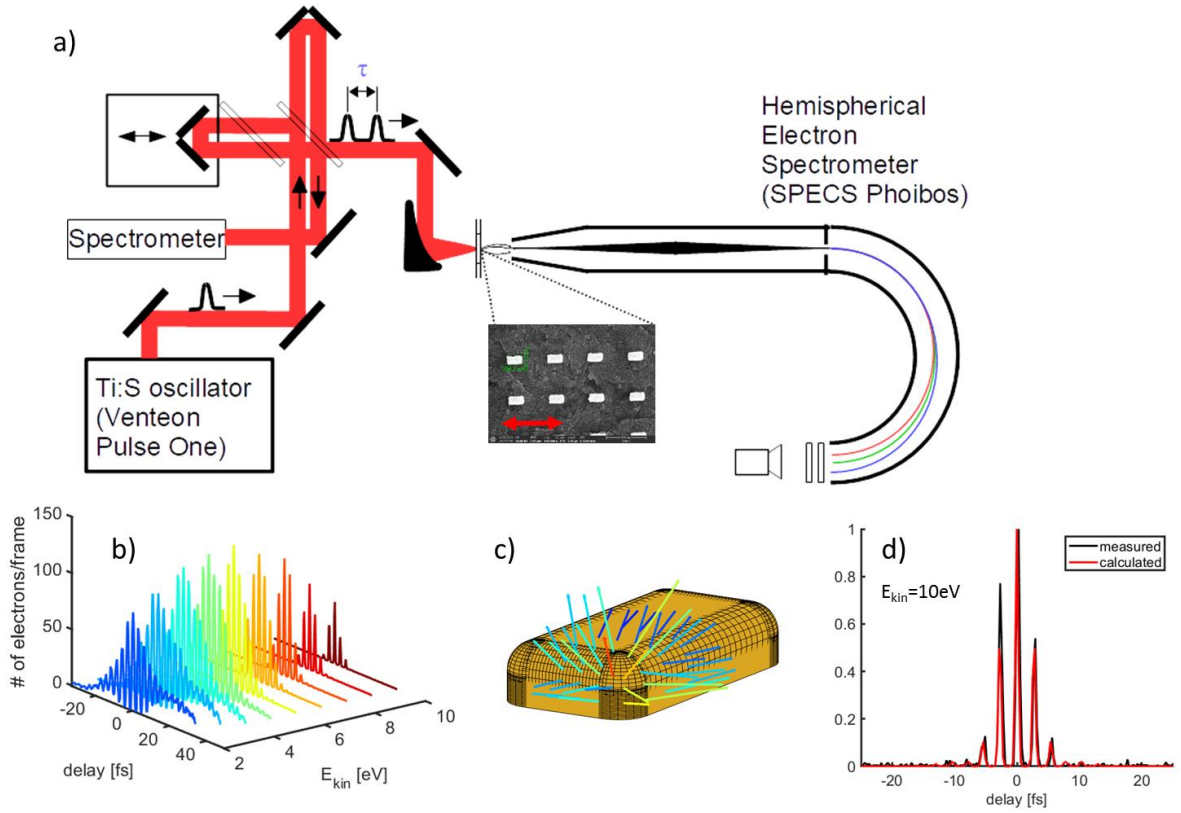

Figure 1: a) Experimental setup user for the electron autocorrelation measurements. b) Measured autocorrelation functions at different photoelectron energy ranges. c) Visualization of surface sites of the investigated nanorod where electrons with different energies are emitted. d) Comparison of measured and simulated autocorrelation traces at the hot-spot.

Our hemispheric electron analyzer allowed us to measure the autocorrelation traces belonging to electrons with different kinetic energy ranges (Fig. 1 b)). Since the electrons with maximum kinetic energy originate from the hot-spots of the nanostructures (where the field enhancement is the largest), with this method we could reveal *the temporal evolution of plasmon field in these hot-spots* on the nanostructures. Nevertheless, these hot-spots represent parts of the investigated samples with few nm spatial dimensions (Fig. 1. c), red arrow) making accessible both *unique temporal and spatial resolution* with our experimental method. To validate the method, we performed FDTD simulations, and got a very good agreement between the measured and calculated autocorrelations at the hot-spot (Fig. 1 d)). First results have already been presented at a conference [T7], and we are working on a manuscript summarizing them.

3) Monitoring plasmon-associated charge dynamics with ellipsometry

The final part of my research focused on different characteristics of the materials hosting surface plasmon polaritons (SPPs). Since the temporal and spatial characteristics of surface plasmons are ultimately determined by the electronic structure of the supporting metal, the built up of plasmon field goes together with the modification of this electronic structure and the optical properties (dielectric function). Ellipsometry is commonly applied for determining optical properties of thin films with very high accuracy; therefore, it is an appropriate candidate for monitoring the plasmon-associated changes in the electronic states of the material.

As a first plasmonic system, we investigated a plasmonic gold layer, where the strongly localized photon absorption due to SPP generation facilitates the emergence of so-called hot-electrons with energy levels that deviate significantly from Fermi-Dirac distribution. In recent years, much attention is focused on these energetic carriers, since hot-electron behavior determines the properties of optically excited materials between the femtosecond and the picosecond time scale. Furthermore, they play an important role in applications across many disciplines including energy conversion, photocatalysis, and photodetection, among others [37].

For our measurements, we followed two experimental approaches to *demonstrate experimentally the spatial- and energy distribution, and the temporal evolution of the SPP mediated hot-electron population in a thin gold film*. In

our first approach, we applied continuous wave (CW) excitation, when the generated SPPs are always present in the system. With this method, we were able to explore the location of the hot-electrons. Pump-probe approach with synchronized ultrafast laser pulses enabled us to determine the dynamics of the excited electron system.

For both experiments, the excitation of SPPs was realized in Kretschmann-geometry involving a glass right angle prism coated with 45 nm gold. SPPs were excited from the backside of the film using either an 808 nm CW diode laser or the 35 fs pump pulses of an amplified Ti:sapphire laser under the angle where k-vector matching is fulfilled. Spectroscopic ellipsometry was applied at the top side of the films, illuminating the samples with a broadband CW light source or with synchronized white light continuum probe for the time-resolved study (schematic drawing of the experimental setup is shown in Fig. 2).

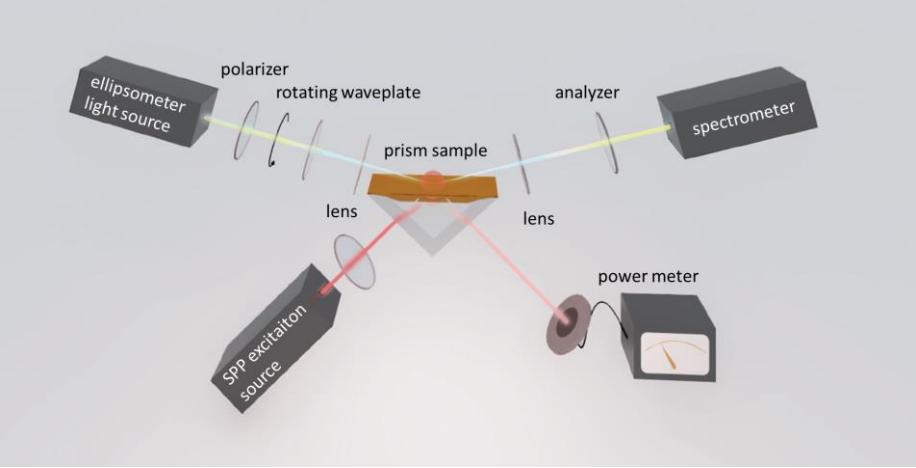

Figure 2: Schematic drawing of the ellipsometric setup. For CW measurements, the light source for SPP excitation is an 808 nm CW diode laser and a broadband Xe lamp drives the ellipsometer setup. For the pump-probe approach, SPPs are excited with 35-fs laser pulses (central wavelength is 800 nm), while the probe pulses used in the ellipsometric setup are synchronized white light pulses produced via supercontinuum generation in a dielectric plate.

In the case of CW excitation of SPPs, ellipsometry revealed - besides the temperature raise of the gold layer - the presence of a surface layer with modified dielectric function accounting for the appearance a non-thermal electron population. The thickness of the non-thermalized layer (<6 nm) clearly shows that hot-electrons are located close to the film surface where plasmon excitation takes place. Changes in the electron occupancies could be retrieved based on the proportionality of the imaginary part of the dielectric function (ε_2) with the electron distribution and the band structure [38]:

$\varepsilon_2(\omega) = \varepsilon_{2,\,intra}(\omega) + \frac{A}{(\hbar\omega)^2}\int_{E_{min}}^{E_{max}} D(\hbar\omega,\, E)\big(1 - f(E)\big)dE$, where $\varepsilon_{2,\,intra}$ is the contribution of the intraband electronic transitions, $D(\hbar\omega,\, E)$ denotes the energy distribution of the joint density of states (EDJDOS), and f(E) describes the electron energy distribution. To determine $\varepsilon_{2,\,intra}$ a Drude function was applied, while to calculate the EDJDOS parabolic band structures were assumed at the L and X points in the Brillouin zone according to [38].

The observed changes and the retrieved electron distributions in the *CW excitation case provide a clear indication of the existence of a hot-electron population with moderately increased energies*. The manuscript summarizing these results is provisionally accepted at Nature Communications (see the manuscript in Appendix I., [39]).

Using the pump-probe ellipsometric approach, we are able to measure the dielectric function of gold at different time instants after the excitation of SPPs corresponding to different excitation states. To describe the changes of the measured dielectric functions, we assumed characteristic electron distributions belonging to the various processes following the SPP excitation. During the first 100fs, the photon absorption perturbs the Fermi-Dirac distribution at energies matching with the excitation energy. Later, a high temperature electron distribution develops. When the energetic electrons interact with the lattice, slight changes are expected near the Fermi energy level accounting for the phonon excitation, and finally the system reaches a thermalized state [40]. By introducing these changes into the electron distribution function (Fig. 3 a)), we can compute the corresponding dielectric function using the equation above. The electron and lattice temperatures applied for these simulations are validated with three-temperature model [41]. The

very good accordance between the measured and calculated curves supports the applicability of our method (Fig. 3 b) and c)).

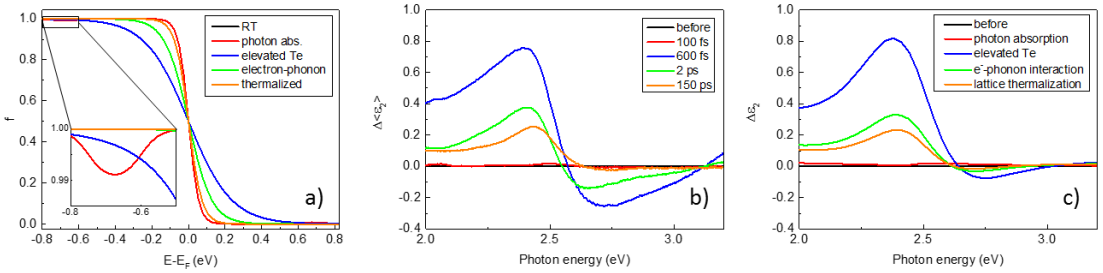

Figure 3: a) Simulated electron distributions belonging to different processes. b) Measured and c) simulated changes in the dielectric function of the plasmonic gold layer.

With our measurements, we could detect the *different stages of the plasmonic system following the SPP excitation and the corresponding electron distributions with ~100 fs temporal resolution*. We presented these results in conference talks [T2, T5, T6], and a manuscript summarizing these results is currently in preparation. These measurements were carried out in collaboration with the ELI Beamlines facility, where the pump-probe ellipsometric setup was available for us. However, to detect the direct signal of the plasmonic hot electrons, we need a better temporal resolution, and as a continuation of this study, we are working on the realization of our own setup driven by a sub-10 fs laser oscillator.

Impact of the research

Regarding the impact of my project, I set the following goals in my proposal: I expected to be able to publish 6-8 refereed international journal publications based on my research, I planned to give oral contributions at international conferences, I aimed to foster the ongoing international collaborations and to establish new ones based on the time-resolved ellipsometry project. I also planned to co-supervise students.

Although the pandemic hindered the planned experimental activities, most of the research goals could be achieved, and I'm convinced that soon we are able to publish those results, where further experiments are needed. The planned budget was spent according to the originally submitted plan. Changes in the purchased tools were already approved during previous report periods.

As a summary, I was able to publish – with my colleagues – *5 international journal publications, one more is provisionally accepted and two others are in preparation*. I gave *3 oral presentations* (*4 other talks* were given by my colleagues participating in the project) and presented *5 posters* on international conferences. We have an ongoing *project with TU Graz*, where my task is to design appropriate plasmonic elements. This would not be possible without the software I purchased from the budget of the project. Furthermore, the ultrafast ellipsometric measurements were carried out in *collaboration with the ELI Beamlines facility in Prague*. A long-term collaboration is expected with them, since after publishing the results on plasmonic gold layers we are planning to move on to plasmonic nanoparticles. This year, I announced *2 PhD positions as co-supervisor* and the two applicants have already started their first semester at the University of Szeged as PhD students on the topics of ultrafast ellipsometry (A. Gera) and plasmon dynamics (L. Tóth).

Finally, I would like to thank again the National Research, Development and Innovation Office for the financial support in the past four years.

References

[1] A. Campion, P. Kambhampati, Chemical Society Reviews 27 (1998) 241.
[2] J. N. Anker, W. P. Hall, O. Lyandres, N. C. Shah, J. Zhao, R. P. Van Duyne. Nature Materials 7 (2008) 442.
[3] D. M. Koller, A. Hohenau, H. Ditlbacher, N. Galler, F. Reil, F. R. Aussenegg, A. Leitner, E. J. W. List, J. R. Krenn. Nature Photonics 2 (2008) 684.

[4] A. L. Falk, F. H. L. Koppens, C. L. Yu, K. Kang, N. de Leon Snapp, A. V. Akimov, M-Ho. Jo, M. D. Lukin, H. Park, Nature Physics 5 (2009) 475.
[5] V. E. Ferry, L. A. Sweatlock, D. Pacifici, H. A. Atwater, Nano Letters 8 (2008) 4391.
[6] S. Tsujino, P. Beaud, E. Kirk, T. Vogel, H. Sehr, J. Gobrecht, A. Wrulich. Applied Physics Letters 92 (2008) 193501.
[7] R. K. Li, H. To, G. Andonian, J. Feng, A. Polyakov, C. M. Scoby, K. Thompson, W. Wan, H. A. Padmore, P. Musumeci. Physical Review Letters 110 (2013) 074801.
[8] J. Vogelsang, J. Robin, B. J. Nagy, P. Dombi, D. Rosenkranz, M. Schiek, P. Groß, C. Lienau. Nano Letters 15 (2015) 4685.
[9] R. G. Hobbs, Y. Yang, A. Fallahi, P. D. Keathley, E. De Leo, F. X. Kärtner, W. S. Graves, K. K. Berggren. ACS Nano 8 (2014) 11474.
[10] M. I. Stockman. Optics Express 19 (2011) 22029.
[11] S. Mazzucco, N. Geuquet, J. Ye, O. Stephan, W. Van Roy, P. Van Dorpe, L. Henrard, and M. Kociak, Nano Lett. 12, 1288 (2012).
[12] O. Nicoletti, F. de la Pena, R. K. Leary, D. J. Holland, C. Ducati, and P. A. Midgley, Nature 502(7469), 80–84 (2013).
[13] E. Marsell, R. Svard, M. Miranda, C. Guo, A. Harth, E. Lorek, J. Mauritsson, C. L. Arnold, H. Xu, A. L'Huillier, A. Mikkelsen, and A. Losquin, Appl. Phys. Lett. 107, 201111 (2015).
[14] M. Aeschlimann, M. Bauer, D. Bayer, T. Brixner, F. J. Garcia de Abajo, W. Pfeiffer, M. Rohmer, C. Spindler, and F. Steeb, Nature 446, 301 (2007).
[15] F. P. Schmidt, H. Ditlbacher, F. Hofer, J. R. Krenn, and U. Hohenester, Nano Lett. 14(8), 4810 (2014).
[16] C. Awada, T. Popescu, L. Douillard, F. Charra, A. Perron, H. Yockell-Lelievre, A.-L. Baudrion, P.-M. Adam, and R. Bachelot, J. Phys. Chem. C 116, 14591 (2012).
[17] M. Cinchetti, A. Gloskovskii, S. A. Nepjiko, G. Schonhense, H. Rochholz, and M. Kreiter, Phys. Rev. Lett. 95, 047601 (2005).
[18] C. Hrelescu, T. K. Sau, A. L. Rogach, F. Jackel, G. Laurent, L. Douillard, and F. Charra, Nano Lett. 11, 402 (2011).
[19] P. Dombi, A. Horl, P. Rácz, I. Márton, A. Trugler, J. R. Krenn, and U. Hohenester, Nano Lett. 13, 674 (2013).
[20] P. Rácz, **Z. Pápa**, I. Márton, J. Budai, P. Wrobel, T. Stefaniuk, C. Prietl, J. R. Krenn, and P. Dombi, Nano Lett. 17(2), 1181 (2017).
[21] J. Budai, **Z. Pápa**, I. Márton, P. Wrobel, T. Stefaniuk, Z. Márton, P. Rácz, and P. Dombi, Nanoscale 10, 16261 (2018).
[22] A. Anderson, K. S. Deryckx, X. G. Xu, G. Steinmeyer, M. B. Raschke. Nano Letters 10 (2010) 2519.
[23] N. Accanto, L. Piatkowski, J. Renger, N. F. van Hulst. Nano Letters 14 (2014) 4078.
[24] S. Onishi, K. Matsuishi, J. Oi, T. Harada, M. Kusaba, K. Hirosawa, F. Kannari. Optics Express 21 (2013) 26631.
[25] E. Marsell, A. Losquin, R. Svärd, M. Miranda, C. Guo, A. Harth, E. Lorek, J. Mauritsson, C. L. Arnold, H. Xu, A. L'Huillier, A. Mikkelsen. Nano Letters 15 (2015) 6601.
[26] A. Kubo, K. Onda, H. Petek, Z. Sun, Y. S. Jung, H. K. Kim. Nano Letters 5 (2005) 1123.
[27] B. J. Nagy, **Z. Pápa**, L. Péter, C. Prietl, J. R. Krenn, P. Dombi, Plasmonics 15 (2020) 335.
[28] P. Dombi, **Z. Pápa**, J. Vogelsang, S. V. Yalunin, M. Sivis, G. Herink, S. Schäfer, P. Groß, C. Ropers, and C. Lienau, Reviews of Modern Physics 92 (2), (2020) 025003.
[29] A. Lübcke, **Z. Pápa**, M. Schnürer, Appl. Sci. 2019, 9, 3636.
[30] B. Banhegyi, L. Peter, P. Dombi, and **Z. Papa**, Applied Optics 61(2) 386 (2022)
[31] G. Herink, D. R. Solli, M. Gulde, and C. Ropers, 2012, Nature **483**, 190.
[32] K. E. Echternkamp, G. Herink, S. V. Yalunin, K. Rademann, S. Schäfer, C. Ropers, 2016, Appl. Phys. B 122, 80.
[33] S. M. Teichmann, et al., 2015, Sci. Rep. 5, 7584.
[34] **Z. Pápa**, P. Sándor, B. Lovász, J. Budai, J. Kasza, Z. Márton, P. Jójárt, I. Seres, Z. Bengery, C. Németh, P. Dombi and P. Rácz, Appl. Phys. Lett. 120, 053103 (2022)
[35] V. G. Kravets, A. V. Kabashin, W. L. Barnes, and A. N. Grigorenko, Chem. Rev., 118 5912 (2018).
[36] **Z. Pápa**, J. Kasza, J. Budai, Z. Márton, Gy. Molnár, and P. Dombi, Appl. Phys. Lett. 2020, 117, 081105
[37] M. L. Brongersma, N. J. Halas, and P. Nordlander, Nat. Nanotechnol. 10, 25 (2015).
[38] T. Heilpern et al., Nat. Comm. 2018, 9, 1853.
[39] J. Budai, **Z. Pápa**, P. Petrik, P. Dombi, Ultrasensitive probing of plasmonic hot electron occupancies, Nat. Comm., provisionally accepted (2022).
[40] Y. Dubi and Y. Sivan, Light: Science & Applications 8, 89 (2019).
[41] M. Conforti, G. Della Valle, Phys. Rev. B 85, 245423 (2012)

List of publications supported by project NKFI FK 128077

Research articles

[1] A. Lübcke, **Z. Pápa**, M. Schnürer, Monitoring of Evolving Laser Induced Periodic Surface Structures, Appl. Sci. 9, 3636 (2019).

[2] B. J. Nagy, **Z. Pápa**, L. Péter, C. Prietl, J. R. Krenn, P. Dombi, Near-field-induced Femtosecond Breakdown of Plasmonic Nanoparticles, Plasmonics 15 335 (2020).

[3] **Z. Pápa**, J. Kasza, J. Budai, Z. Márton, Gy. Molnár, and P. Dombi, Tuning plasmonic field enhancement and transients by far-field coupling between nanostructures, Appl. Phys. Lett. 117, 081105 (2020).

[4] **Z. Pápa**, P. Sándor, B. Lovász, J. Budai, J. Kasza, Z. Márton, P. Jójárt, I. Seres, Z. Bengery, C. Németh, P. Dombi and P. Rácz, Control of Plasmonic Field Enhancement by Mode-mixing, Appl. Phys. Lett. 120, 053103 (2022).

[5] B. Banhegyi, L. Peter, P. Dombi, and **Z. Pápa**, Femtosecond LIPSS on indium-tin-oxide thin films at IR wavelengths, Applied Optics 61(2) 386 (2022) .

[6] J. Budai*, **Z. Pápa***, P. Petrik, P. Dombi, Ultrasensitive probing of plasmonic hot electron occupancies, Nat. Comm., provisionally accepted (2022) – *equal contribution of the authors

Conference talks

[T1] **Z. Pápa**, Monitoring electron occupancies in a gold film upon plasmon excitation, ELI-Beamlines User Workshop, October 2020, Praha, Czech Republic (online) – *invited talk*

[T2] **Z. Pápa**, Ultrafast probing of plasmonic hot electron lifetimes, WSE 11 conference, Steyr, 2021.

[T3] J. Budai, Optical Probing of Plasmonic Hot Electron Occupancies, WSE 11 conference, Steyr, 2021.

[T4] P. Dombi, Optical Probing of Plasmonic Hot Electron Occupancies, META Conference, online, 2021.

[T5] **Z. Pápa**, Ultrafast Probing of Electron States after Plasmon Excitation - Attochem (2nd Annual Workshop of Attochem COST Action), October 13-15, 2021 (online) – *invited talk*

[T6] J. Budai, Ellipsometry giving insight into plasmonic electron distributions, ICSE9, 2022 (online) - *keynote talk*

[T7] P. Sándor, Few femtosecond plasmon transients probed with nm-scale sensitivity, SPIE Photonics Europe, 2022 Strassbourg, France

Conference posters

[P1] **Z. Pápa**, J. Csontos, P. Dombi, J. Budai, Ellipsometry of Surface Plasmons, 3rd ELIps User Workshop, 2018

[P2] **Z. Pápa**, J. Csontos, P. Dombi and J. Budai, Ultrafast Nanoplasmonic Probing of the Dielectric Response of Metals, Ultrafast Phenomena Conference, 2020

[P3] J. Budai, **Z. Pápa**, J. Csontos, P. Dombi, Ellipsometry of Surface Plasmons, SPP9, 2019

[P4] **Z. Pápa**, P. Dombi, J. Budai, Ultrafast Probing of Plasmonic Hot-electron Occupancies, MUST conference, 2022

[P5] **Z. Pápa**, P. Sándor, B. Lovász, J. Budai, P. Dombi and P. Rácz, Control of Plasmonic Field Enhancement by Mode-mixing, Ultrafast Phenomena Conference, 2022

Appendix I. Manuscript of the CW ellipsometric results

Ultrasensitive probing of plasmonic hot electron occupancies

J. Budai[1,2*], Z. Pápa[1,3], P. Petrik[4], P. Dombi[1,3]

1 ELI-ALPS, ELI-HU Non-Profit Ltd., Szeged, H-6728, Hungary

2 Department of Optics and Quantum Electronics, University of Szeged, Szeged, H-6720, Hungary

3 Wigner Research Centre for Physics, Budapest, H-1121, Hungary

4 Institute of Technical Physics and Materials Science, Centre for Energy Research, Budapest, H-1121, Hungary

* corresponding author: Judit Budai, judit.budai@eli-alps.hu

Abstract

Non-thermal and thermal carrier populations in plasmonic systems raised significant interest in contemporary fundamental and applied physics. Although the theoretical description predicts not only the energies but also the location of the generated carriers, the experimental justification of these theories is still lacking. Here, we demonstrate experimentally that upon the optical excitation of surface plasmon polaritons, a non-thermal electron population appears in the topmost domain of the plasmonic film directly coupled to the local fields. The applied all-optical method is based on spectroscopic ellipsometric determination of the dielectric function, allowing us to obtain in-depth information on surface plasmon induced changes of the directly related electron occupancies. The ultrahigh sensitivity of our method allows us to capture the signatures of changes induced by electron-electron scattering processes with ultrafast decay times. These experiments shed light on the build-up of plasmonic hot electron populations in nanoscale media.

Within the realm of plasmonics, it is of great interest to probe matter on the level of electron occupancies. The strong localization of plasmon assisted photon absorption facilitates the

emergence of so-called hot electrons within a few tens of femtoseconds after plasmon excitation with energy levels that deviate significantly from Fermi-Dirac distribution. In recent years, much attention is focused on the ultrafast generation of these hot carriers, due to their fundamental role in emerging applications such as nanoscale electron emitters for ultrafast probing of matter [1], construction of nanoscale optical circuitry [2-4], hot electron-enhanced photocatalysis, photovoltaics and sensorics [5-7]. Regarding the feasibility of such devices, the development of theoretical and experimental methods to determine the energy distribution of hot electrons and to identify dominant mechanisms is essential. For localized plasmons in nanoparticles, Govorov and coworkers studied the generation and injection of plasmonic carriers from optically excited metal nanocrystals and they found that for nanocrystal sizes larger than 20 nm, the energies of excited electrons are close to the Fermi level [8]. The detailed theoretical study of Dubi et al. also pointed out that assuming continuous excitation, it is thermalization that dominantly determines electron distributions [9]. For a thin gold film that supports surface plasmon polaritons (SPPs), reflectometry experiments of Takagi et al. revealed slight differences in plasmonic response and temperature modulation spectra [10]. These differences may originate from electrons exhibiting a broader energy distribution belonging to the SPP mediated case, as shown in a comparative study of Heilpern et al. on photon absorption processes with and without SPP excitation via time-resolved reflectometry [11]. In a similar model system, Reddy et al. observed energetic electrons up to 0.3 eV based on transport measurements from single-molecule junctions [12]. However, all of these recent studies have focused on the energy distribution of the hot carriers, and only limited attention has been paid to the effect of the surface-bound nature of SPPs on the location of hot electron population in the depth of the film.

There are different SPP related phenomena exhibiting an in-depth variation. Upon SPP generation, a significant part of the electromagnetic energy of the incoming field is transformed to the kinetic energy of free carriers resulting in the longitudinal oscillation of electrons. The screening of the locally excess/absent negative charge carriers is described by the Thomas-Fermi screening, or more

recently via Friedel-oscillation both predicting that free carriers are confined within a few-nm vicinity of the surface [13]. This means that the excitation energy is dominantly concentrated near the surface [14]. During this process, known as SPP excitation, a collective oscillation of charges builds up with a confined, exponentially decaying electric field exhibiting also a field enhancement effect [15-17]. The volume of the SPP mode can be characterized by a penetration depth of ~10 nm into the metal. Within this volume, SPPs contribute to hot electron generation by various absorption mechanisms [18]. Phonon and defect assisted absorption occurs throughout the entire volume of the SPP mode in the metal, while carrier generation via Landau damping takes place right at the surface [19]. These local phenomena associated to SPPs affect the spatial distribution of hot electrons which is a fundamental question regarding hot-electron enabled devices. Although these theoretical results predict the existence of non-thermal electrons localized close to the sample surface, its experimental demonstration is still lacking. Thus, it is essential to develop an experimental method that is sensitive enough to explore the in-depth distribution of the electrons and identify the possibly appearing subdomains experimentally (referred to as layers of the plasmonic thin film throughout this paper) exhibiting different electron distribution functions.

Here, we demonstrate experimentally the existence of an electron population with high energies compared to the bulk of the gold film having a non-thermal nature; and more importantly, we also reveal its spatial extent near the surface of a plasmonic gold film. For the ultrasensitive probing of plasmonic electron occupancies we developed a spectroscopic ellipsometry method, enabling the detection of the energy distribution of the generated electrons.

In ellipsometry, measured data carry information about the changes in the polarization state of light upon reflection, which are quantified by two ellipsometric angles, conventionally called as Ψ and Δ, describing the relative amplitude and phase change of the reflected light. As these two quantities are in close correlation with the complex dielectric function, ellipsometry provides simultaneous access to the absolute value of both the real (ε_1) and imaginary parts (ε_2) of the dielectric function. As electron occupancies change during the photoexcitation of metals, so does the dielectric function

[20]. This means that it is possible to retrieve electron occupancies related to plasmon excitation and decay by measuring the dielectric function of the plasmonic system in a highly sensitive way. Another advantage of this approach is its ultrahigh sensitivity to surface phenomena [21] and the in-depth information about the dielectric function of the layers constituting the gold film. By exploiting these features of ellipsometry, we could reveal that continuous wave (cw) excitation holds fingerprints of several plasmon-related effects simultaneously.

Results

Experiments

For the excitation of SPPs, we applied the Kretschmann geometry involving a glass right-angle prism coated with 45 nm gold by thermal evaporation (see Fig. 1 and Methods section).

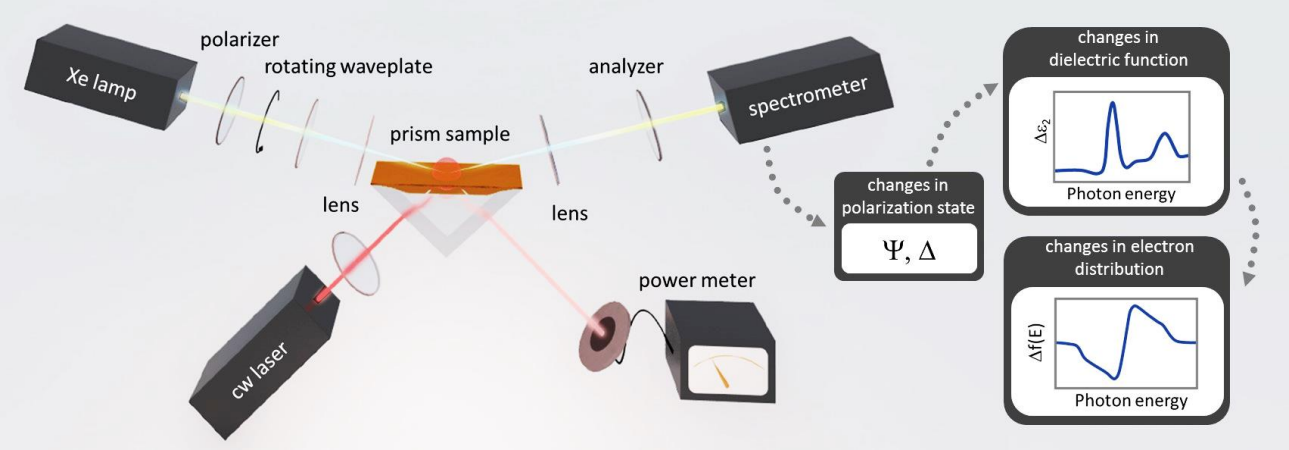

Fig. 1. Experimental setup for ultrasensitive probing of plasmonic hot electrons with spectroscopic ellipsometry. SPPs are excited by a cw laser at the resonant angle of incidence from the backside, while ellipsometric data is recorded on the gold-air interface with white-light probing from the top. These measurements are capable of accessing the dielectric function of the investigated system, the changes of which are in close correlation with the electron distribution function.

We applied different laser intensities for exciting SPPs, and, as a unique feature, monitored the changes in the optical properties of the plasmonic system by recording the ellipsometric response with and without plasmon excitation (i.e. at the on and off states of the cw laser that excites plasmons, respectively), the latter for reference. Although the ellipsometric angles of the non-plasmonic geometry and the one inducing SPPs differ only very slightly (see Supplementary Information), notable deviations can be identified in the difference signal (presented in Fig. 2 a) and

b) with blue curves noted as Ψ_{EXC}-Ψ_{REF} and Δ_{EXC}-Δ_{REF}). Though the amplitude of the emerging peaks increases with increasing laser power, their position can not be directly correlated with the excitation energy (1.53 eV), as one would expect from classical spectroscopic methods. Instead, as a matter of fact, it is related to the structure of dielectric function near the spectral regions where it changes rapidly (photon energies of band to band transitions occurring as structures in the first derivative of ε_2, see inset of Fig. 2). This clearly indicates that the observed differences in the ellipsometric curves originate from the changes in the dielectric function, with the change clearly being induced by SPP generation. To follow these trends quantitatively, it is necessary to perform a detailed modeling.

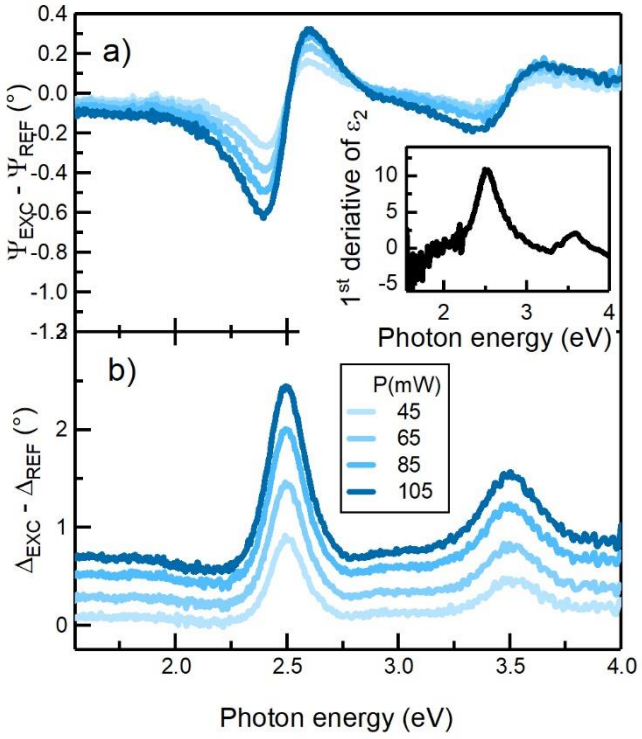

Fig. 2. a) and b) Measured ellipsometric difference curves for surface plasmon polariton excitations at different laser powers. Note that delta values (b)) are offset for better visibility. The inset shows the first derivative of the imaginary part of the dielectric function of gold determined in this study. Peak positions in the ellipsometric curves correspond to rapid changes in the dielectric function of gold, i.e. peaks in its first derivative.

Retrieving the dielectric function

Ellipsometric modeling includes the description of the layer structure of the investigated system, and more importantly the optical behavior of each layer. In our cw excitation case, one would expect that the most prominent effect is the temperature rise of the whole film, due to the mechanisms accompanying the decay/absorbance of SPPs. If it is only the temperature that initiates measurable changes in the ellipsometric response of the sample upon SPP excitation, then a model system containing a single homogeneous gold layer with temperature-dependent dielectric function should describe our data perfectly [23]. For determining the temperature-dependent dielectric function of gold, we performed ellipsometric measurements on a uniformly heated sample (containing the same gold layer as the gold coated prism), without SPP excitation (details about ellipsometric modeling is provided in Supplementary Information). The resulting temperature dependent dielectric function datasets were used to describe ellipsometric data gained upon SPP excitation. When calculating the deviation of the modeled ellipsometric data and the measured ones, distinct peaks occur – see e.g. the difference in the delta curves in Fig. 3.a) -, clearly indicating that solely the temperature rise is not able to sufficiently describe the measured changes. In other words, there must be other contributions beside the temperature increase of the plasmonic thin film originating from the absorption of SPPs near the surface (non-thermal effects).

To prove that this additional non-thermal contribution belongs exclusively to SPP excitation, we performed measurements by illuminating the sample from the top, so that plasmon generation is excluded. It can be shown that the ellipsometric difference curves belonging to top illumination behave similarly to the ones recorded on uniformly heated sample, and are clearly distinguishable from the plasmon mediated case (Supplementary Information). This supports that SPP related effects have to be taken into account to describe the observed changes.

The direct effects of the presence of SPPs can be twofold. i) Nonlinear effects can take place if the enhanced near-fields exceed a certain value [24], and ii) the occupancy of the electronic states is altered upon plasmon excitation [9, 11]. By determining the local field distribution, we can exclude the nonlinear effects caused by the presence of enhanced plasmonic near-fields, as the emerging

electric near-fields are not high enough (Supplementary Information). Focusing onto the modified occupancy of the electronic states, we have to take into account that SPP-related phenomena are bound to the surface. Therefore, the non-thermal electron distributions associated to SPPs affecting the dielectric function might be present only in the topmost portion of the gold film, similarly to the penetration effect already noted for direct photon absorption by [11]. Furthermore, due to the energy dependent characteristic times of the decay processes, we can expect that electrons with different energy levels exhibit different spatial patterns within the gold film, and the more energetic, non-thermal electrons are located close to the sample surface [6]. As a consequence, we divided the gold film into two layers in our model, i) a lower layer with increased temperature exhibiting thermal electron distribution (thermalized layer), described via the temperature dependent optical model as before, and ii) an upper layer accounting for the non-thermal electron distribution due to the appearance of SPPs and the associated hot electron generation (non-thermalized layer). When calculating the deviation of the measured and simulated ellipsometric curves, the distinct peaks occurring earlier in the case of the simple thermal model diminish (Fig. 3 a)). This plot clearly shows that the model properly describes the measured data, and supports the presence of the non-thermalized surface layer in accordance with the theoretical predictions.

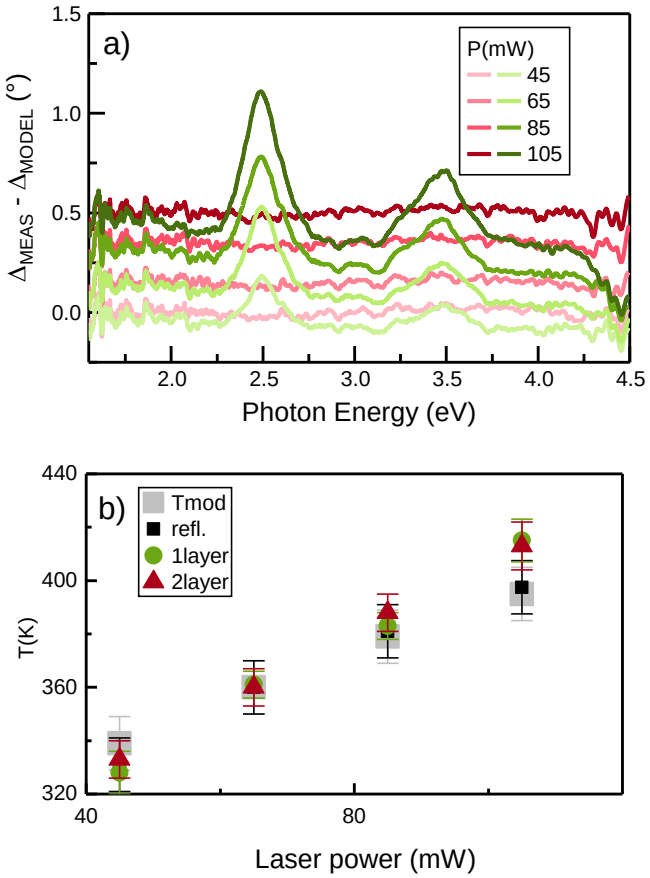

Figure 3. a) Comparison of the measured and modeled ellipsometric data. Green curves belong to the single layer model, where the appearing distinct peaks provide a clear indication that this simple model is not able to describe the measured changes sufficiently. Red curves with no modulation belong to the two-layer model, which reproduces perfectly the measurements. b) Temperature of the thin film hosting the SPPs as a function of laser power applied for SPP excitation. Black, green, red and grey symbols represent the temperature originating from reflectivity measurements, from the ellipsometric model considering a single layer with elevated temperature, from the ellipsometric model considering two layers, and from temperature calculations, respectively.

Both modeling procedures allowed us to estimate the temperature of the gold film, values of which are shown in Fig. 3 b) with green circles for the purely thermal model (single layer model) and red triangles for the non-thermal modeling (two-layer model). For the latter case, the temperature for the thermalized part of the gold film is shown. We compared these temperature values with the results of two other temperature estimations, i) an experimental method based on the reflectivity changes of the gold film and ii) temperature calculations. Determining the local temperature of metal thin films is not straightforward, therefore we applied the method of measuring the

temperature dependent changes in the reflectivity of metals in the visible spectral range [22], which can be applied by means of the ellipsometric measurements as well (see Supplementary Information). This way, we could determine the temperature of the gold film under SPP excitation (Fig. 3 b), black squares). Thermal modeling carried out with COMSOL Multiphysics (see Supplementary Information) supports these values, as evidenced by Fig. 3 b), grey squares. As a further evidence of the soundness of our modeling, temperature values of all four approaches coincide within the error bars.

In the final section of the paper, we are focusing on the conclusions drawn from the two-layer model and their interpretation. As the main results of the ellipsometric analysis, the thickness and the dielectric function of the non-thermalized and thermalized layers became also available. The thickness of the non-thermalized layer increases with the applied laser intensity from 4 nm to 6 nm corresponding to the spatial extent of the hot electron population. Here we have to note, that though our modeling would suggest a step-like transition between the spatial regions of non-thermal and thermal carriers, in reality the boundary between these regions follows a continuous transition. Such continuous change in the electron distributions could have been mimicked as a gradient with several sublayers but such description would result in a large number of fitting parameters and thus large uncertainties. To avoid these, we applied the simplest, step-like model, which – based on the results – already provides a clear indication that non-thermal carriers are located close to the surface of the gold layer in a nanometric volume.

When comparing the dielectric function of the thermalized and non-thermalized layers, minor differences can be observed in the intraband transition part of the spectrum (below 1.7 eV) with major differences occurring in the interband transition domain. In the intraband domain, the imaginary part of the dielectric function at the surface is slightly increased as compared to that of the thermalized part (Fig. 4. a)), while in the interband region, there are multiple features with the most prominent peak appearing in the difference curves around 2.3 eV. These features become wider as the applied laser intensity increases. To gain insight into the origin of these differences, first

we applied different excitation geometry, which allowed us to exclude the contribution of nonlocal effects [24-26] (for details see Supplementary Information). As a next step, we calculated the dielectric function of the two layers based on its proportionality with the joint density of electron states and electron occupancies. Practically, we considered different transitions near the X and the L points of the Brillouin-zone and different electron occupancies (f(E)) to reproduce the most prominent peak of the ε_2 difference curves ($\Delta\varepsilon_2$). Description of other features of the $\Delta\varepsilon_2$ curves corresponding to further transitions are beyond the scope of this work. To avoid any presumption regarding the $\Delta f(E)$ curves, we introduced a spline-based fitting method capable of the direct inversion of the $\Delta\varepsilon_2$ curves (for details see Supplementary Information). Fitting of the 2.3 eV peak of the $\Delta\varepsilon_2$ curves and the resulting $\Delta f(E)$ curves are presented in Fig. 4. along with the $\Delta f(E)$ curve belonging to two Fermi-Dirac distributions having temperatures of 400K and 550K as a reference, for the corresponding purely thermal $\Delta\varepsilon_2$ curve see Supplementary Information.

According to the curves in Fig. 4. b), we could identify changes in the electron distribution only in the vicinity of the Fermi-level in all cases, suggesting that the number of energetic hot charge carriers is very low in accordance with Ref. [8]. With increasing laser power, the $\Delta f(E)$ curves differ from the thermal distribution to an increasing extent: the curves become broadened with a slight shift in their maxima. Both broadening and spectral shift can be the consequence of an increased electron temperature of the top layer taking into account an elevated background temperature. An increase in the electron temperature increases the plasma frequency and reduces the electron scattering lifetimes [28], resulting in slightly higher infrared absorption and also influencing the occupancies in the vicinity of the Fermi-level (Fig. 4. b)) [11]. However, the extent of the broadening (mainly for the higher laser powers) indicates a more distorted electron distribution. This is the spectral fingerprint of an additional hot electron population with energy levels up to 0.4 eV measured from the Fermi level. Upon the generation of SPPs with photons of $\hbar\omega$ energy, their phonon and surface assisted absorption results in charge carriers with average excess energies of $\hbar\omega/2$, electron-electron scattering assisted absorption generates electrons of lower average energy, namely $\hbar\omega/4$ [14]. This

energy is equal to 0.4 eV in our case, indicating that electron-electron scattering assisted absorption is the dominant mechanism. Interband absorption would excite electrons just above the Fermi energy, but this process is not considered here due to the low photon energy applied (ħω=1.53 eV).

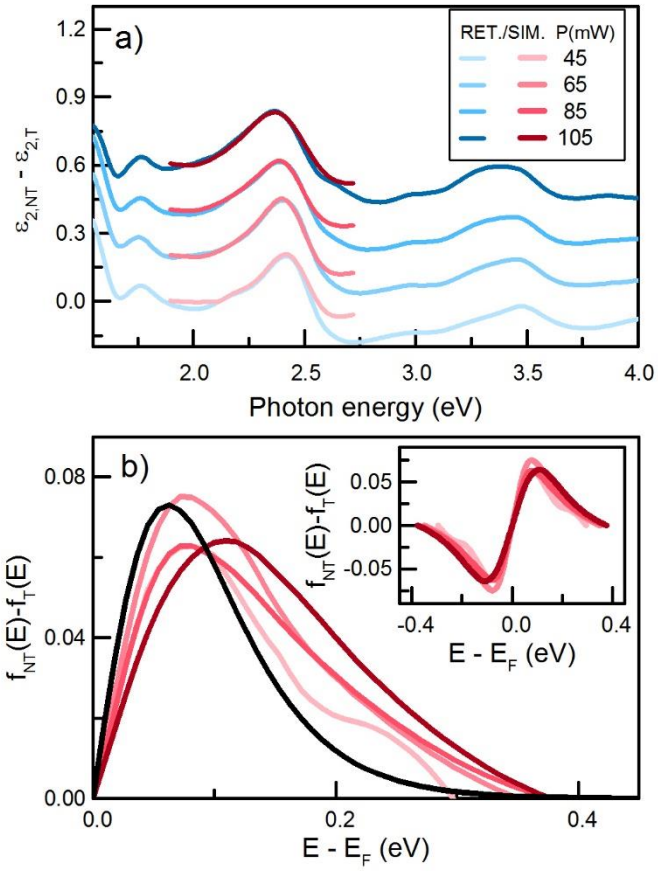

Fig. 4. a) Retrieved (blue set of curves) and simulated (red set of curves) differences between the dielectric function of the non-thermalized top layer (NT) and the thermalized part (T) of the gold film and b) the corresponding changes in the electron occupancies above Fermi-level. The inset shows Δf(E) in the whole affected energy range. For comparison, the difference of two Fermi-Dirac distributions belonging to ΔT= 275K is presented with a dashed grey line.

The retrieved energy distribution of electrons in the thermalized and non-thermalized layers can be interpreted as follows. At the surface, SPPs are continuously generated, and they are absorbed within a few tens of femtoseconds via different mechanisms, resulting in electrons (and holes) of elevated energies. These energetic electrons thermalize via electron-electron and electron-lattice scattering, approaching an equilibrium, i.e. reducing the electron energies and increasing the lattice temperature of the whole film as we see in the thermalized part of the gold film. More interestingly, our observations provide a clear indication of an additional hot-electron population close to the film

surface within a nanometric range depending on the excitation intensity. The extent of this non-thermalized layer coincides with the expected location of hot electron generation via Landau damping which would result in electron energies up to 0.8 eV ($\hbar\omega/2$) with respect to the Fermi level. However, since electron-electron scattering probability is strongly dependent on energy, - namely electron collision rate is much larger for more energetic electrons [9], - less energetic electrons remain in the system giving rise to the observed electron distribution in the 0.4 eV vicinity of the Fermi level.

In summary, we could detect the development of a hot electron population in a nanometric surface layer induced by the continuous excitation and absorption of SPPs. The signatures of these transient electronic states of hot electrons were revealed with the help of spectroscopic ellipsometry. Taking advantage of the in-depth information extracted with our method, we could decouple the heating effect of plasmon decay from the direct effect of SPPs on the occupancies of electronic states. This enabled us to directly probe and demonstrate the presence of plasmonic hot charge carriers at the surface. The method demonstrated here also opens the pathway toward ultrafast time-resolved investigations of hot electron dynamics with ultrasensitive optical tools, i. e. with ultrafast spectroscopic ellipsometry.

Methods

Experimental methods. For the excitation of SPPs, we applied the Kretschmann geometry involving a right-angle glass prism coated with 45 nm gold layer prepared in a custom-made Pfeiffer Vacuum Classic 570 coating chamber by thermal evaporation, under the following conditions: The chamber was pumped by a HiPace 1500 turbopump with 1450 l/sec. The base pressure was $2x10^{-5}$ mbar (1.5×10^{-5} Torr). The source to substrate distance was 35 cm. A planetary substrate holder was used to reach homogeneous film thickness. A 70 mm long by 17 mm wide by 0.5 mm thick (Umicore) tungsten boat was used with 1g 99.99% Au pellets as source material. The boat was heated by a 4V, 1000A power supply. The deposition rate was 10 Å/s. With these parameters the rms roughness of our gold layer is 0.6 nm (measured with atomic force microscope), which was taken into account in

the analysis. Compared to Norris recipe [30], the parameters are very similar except for the base pressure, which was limited by the chamber properties. The differences in base pressure explain our slightly larger rms roughness value as compared to that measured by Norris and coworkers. They reported 0.3 nm rms roughness 10 Å/s deposition rate and 3×10^{-8} Torr base pressure, and 0.4 nm rms roughness for 0.5 Å/s and 2×10^{-6} Torr.

The list of the different phases/layers of our measured system is shown in Table 1.

Phase/layer	Thickness
air	∞
roughness	0.6 nm
gold – non-thermal	4-6 nm
gold – thermal	39-41 nm
chromium	2 nm
glass substrate	∞

Table S1. Different phases/layers of the investigated plasmonic system and their thicknesses.

SPPs were excited from the backside of the film using an 808 nm (1.53 eV) cw diode laser illuminating the sample under the angle of a sharp SPP resonance. Simultaneously, spectral fingerprints of SPP-related changes were monitored by means of spectroscopic ellipsometry (Semilab SE1000, rotating compensator spectroscopic ellipsometer), illuminating the sample from the top side (i.e. directly the air-gold interface) with a continuous, broadband light source (Xe lamp, applied photon energy range: 1.55-4 eV) under 55° and 65° angles of incidence. The light from the Xe lamp is in a well-defined polarization state being set by a fixed polarizer and the rotating waveplate/compensator. The polarization state after reflection from the sample is monitored by another fixed polarizer, called analyzer.

Computational methods. Different ellipsometric models were used to describe the actual properties of the sample under the various excitation conditions. These are detailed in the Supplementary Information, here we provide only a short overview. To determine the thickness of our gold film we

applied a five-component model consisting of BK7 glass, Cr adhesion layer, gold layer, surface roughness (determined by atomic force microscopy) and air. We described the optical properties of the gold layer and the surface roughness layer with a spline-based optical model, and with effective medium approximation, respectively. Besides its dielectric function, spline-based model provided also the thickness of the gold film. Modeling of the gold film hosting SPPs were carried out with i) a single layer model, handling the gold as a homogeneous film using the retrieved temperature dependent optical properties, while ii) the 2-layer modeling applying the temperature dependent optical data to describe the thermalized layer and the optical properties of the non-thermalized layer were described using again the spline based optical model. The total thickness of the layer system was kept fixed, and several iteration steps were done to find the optimal thickness of the non-thermal layer showing the best fit.

To reveal the origin of the differences found when comparing the non-thermalized and thermalized layers' dielectric constants, we calculated the dielectric function based on its proportionality with the joint density of electron states and electron occupancies [11]:

$$\varepsilon_2(\omega) = \varepsilon_{2,\,intra}(\omega) + \frac{A}{(\hbar\omega)^2}\int_{E_{min}}^{E_{max}} D(\hbar\omega,\, E)\big(1 - f(E)\big)\, dE, \qquad (1)$$

where $\varepsilon_{2,intra}$ is the contribution of the intraband electronic transitions, $D(\hbar\omega,\, E)$ denotes the energy distribution of the joint density of states (EDJDOS), *f(E)* describes the electron energy distribution. Constant *A* was determined based on a fitting to the dielectric function measured in this study at room temperature without laser excitation. To determine $\varepsilon_{2,intra}$ a Drude function was applied [28], while to calculate the EDJDOS parabolic band structures were assumed at the L and X points in the Brillouin zone according to [11, 29]. The changes in the electron distribution function were modeled with a spline-based fitting algorithm avoiding any a priori assumptions.

Data availability. The data that support the findings of this study are available from the corresponding author on reasonable request.

References

[1] P. Dombi, Z. Pápa, J. Vogelsang, S. V. Yalunin, M. Sivis, G. Herink, S. Schäfer, P. Groß, C. Ropers, and C. Lienau, "Strong-field nano-optics," Rev. Mod. Phys. **92**, 025003 (2020).
[2] F. Krausz and M. I. Stockman, "Attosecond metrology: from electron capture to future signal processing," Nat. Phot. **8**, 205 (2014).
[3] C. Karnetzky, P. Zimmermann, C. Trummer, C. Duque Sierra, M. Wörle, R. Kienberger, A. Holleitner, "Towards femtosecond on-chip electronics based on plasmonic hot electron nano-emitters," Nat. Comm. **9**, 2471 (2018).
[4] C. I. Evans and D. Natelson, "Remote Excitation of Hot Electrons via Propagating Surface Plasmons," J. Phys. Chem. C **123**, 10057 (2019).
[5] X. Zhang, Y. Chen, R.-S. Liu, D. P. Tsai, "Plasmonic photocatalysis," Rep. Prog. Phys. **76**, 046401 (2013).
[6] M. L. Brongersma, N. J. Halas, and P. Nordlander, "Plasmon-induced hot carrier science and technology," Nat. Nanotechnol. **10**, 25 (2015).
[7] G. Baffou, R. Quidant, "Nanoplasmonics for chemistry," Chem. Soc. Rev. **43**, 3898–3907 (2014).
[8] A. O. Govorov, H. Zhang, and Y. K. Gun'ko, "Theory of Photoinjection of Hot Plasmonic Carriers from Metal Nanostructures into Semiconductors and Surface Molecules," J. Phys. Chem. C **117**, 16616−16631 (2013).
[9] Y. Dubi and Y. Sivan, ""Hot" electrons in metallic nanostructures—non-thermal carriers or heating?," Light: Science & Applications **8**, 89 (2019).
[10] K. Takagi, S. V. Nair, J. Saito, K. Seto, R. Watanabe, T. Kobayashi, and E. Tokunaga, "Plasmon Modulation Spectroscopy of Noble Metals to Reveal the Distribution of the Fermi Surface Electrons in the Conduction Band," Appl. Sci. **7**, 13 (2017).
[11] T. Heilpern, M. Manjare, A. O. Govorov, G. P. Wiederrecht, S. K. Gray, and H. Harutyunyan, "Determination of hot carrier energy distributions from inversion of ultrafast pump-probe reflectivity measurements," Nat. Comm. **9**, 1853 (2018).
[12] H. Reddy, K. Wang, Z. Kudyshev, L. Zhu, S. Yan, A. Vezzoli, S. J. Higgins, V. Gavini, A. Boltasseva, P. Reddy, V. M. Shalaev, E. Meyhofer, "Determining plasmonic hot-carrier energy distributions via single-molecule transport measurements," Science **369**, 423 (2020).
[13] A. Trügler, Optical Properties of Metallic Nanoparticles, Springer Series in Materials Science (Springer International Publishing Switzerland, 2016).
[14] J. B. Khurgin, "Hot carriers generated by plasmons: where are they generated and where do they go from there?," Faraday Discuss. **214**, 35 (2019).
[15] P. Dombi, A. Horl, P. Rácz, I. Márton, A. Trügler, J. R. Krenn, U. Hohenester, "Ultrafast Strong-Field Photoemission from Plasmonic Nanoparticles," Nano Letters **13**, 674 (2013).
[16] P. Rácz, Z. Pápa, I. Márton, J. Budai, P. Wróbel, T. Stefaniuk, C. Prietl, J. R. Krenn, P. Dombi, "Measurement of Nanoplasmonic Field Enhancement with Ultrafast Photoemission," Nano Letters **17**, 1181 (2017).
[17] J. Budai, Z. Pápa, I. Márton, P. Wróbel, T. Stefaniuk, Z. Márton, P. Rácz, P. Dombi, "Plasmon–plasmon coupling probed by ultrafast, strong-field photoemission with <7 Å sensitivity," Nanoscale **10**, 16261 (2018).
[18] J. B. Khurgin, "How to deal with the loss in plasmonics and metamaterials," Nat. Nanotechnol. **10**, 2 (2015).
[19] J. B. Khurgin, "Ultimate limit of field confinement by surface plasmon polaritons," Faraday Discuss. **178**, 109 (2015).
[20] M. Cardona, Fundamentals of Semiconductors, 3rd edition (Springer, Berlin, 2005).

[21] T.W.H. Oates, H. Wormeester, H. Arwin, “Characterization of plasmonic effects in thin films and metamaterials using spectroscopic ellipsometry,” Progr. in Surf. Sci. **86**, 328 (2011).
[22] T. Favaloro, J.-H. Bahk and A. Shakouri, “Characterization of the temperature dependence of the thermoreflectance coefficient for conductive thin films,” Rev. Sci. Ins. **86**, 024903 (2015).
[23] M. Magnozzi, M. Ferrera, L. Mattera, M. Canepa, F. Bisio, “Plasmonics of Au nanoparticles in a hot thermodynamic bath,” Nanoscale **3,** 1140 (2019).
[24] R. W. Boyd, Z. Shi, and I. De Leon, “The third-order nonlinear optical susceptibility of gold,” Opt. Comm. **326**, 74 (2014).
[25] T. V. Teperik, P. Nordlander, J. Aizipurua, and A. G. Borisov, “Quantum effects and nonlocality in strongly coupled plasmonic nanowire dimers,” Opt. Express, 21, 27306, (2013).
[26] D. Forcella, C. Prada, and R. Carminati, “Causality, Nonlocality, and Negative Refraction,” Phys. Rev. Lett. 118, 134301, (2017).
[27] P. J. Feibelman, “Surface Electromagnetic Fields,” Progress In Surface Science, Vol. 12, pp. 287-408, 1982
[28] H. Reddy, U. Guler, A. V. Kildishev, A. Boltasseva, and V. M. Shalaev, “Temperature-dependent optical properties of gold thin films,” Opt. Mat. Exp. **6**, 2776 (2016).
[29] N. E. Christensen and B. O. Seraphin, „Relativistic band calculation and the optical properties of gold,” Phys. Rev. B **4**(10), 3321 (1971).
[30] K. M. McPeak, S. V. Jayanti, S. J. P. Kress, S. Meyer, S. Iotti, A. Rossinelli, D. J. Norris, “Plasmonic Films Can Easily Be Better: Rules and Recipes,” ACS Phot. **2**, 326 (2015).

Acknowledgements

We would like to thank V. Hanyecz for her help in sample preparation, V. Hanus for discussions, and T. Smausz and B. Hopp for their support in implementing the experiments. SEMILAB Ltd. is highly appreciated for making available the SE1000 ellipsometer. The ELI-ALPS project (GINOP-2.3.6-15-2015-00001) is supported by the European Union and co-financed by the European Regional Development Fund. The authors received funding from the National Research, Development and Innovation Office of Hungary (grants VEKOP-2.3.2-16-2017-00015, FK 128077, K-131515, KKP-137373 and 2018-1.2.1-NKP-2018-00012).

Author contributions

J. B. and Z. P. developed the concept of the experiments. J. B., Z. P., and P. P. performed the experiments. J. B. developed the theoretical models and performed the calculations. J. B., Z. P. and P. D. analyzed results and prepared the manuscript. J. B. and Z. P. contributed equally.

Competing interests

The authors declare no competing interests.